nature COMMUNICATIONS

ARTICLE

Received 6 Aug 2014 | Accepted 21 Jan 2015 | Published 24 Feb 2015

DOI: 10.1038/ncomms7346

An extreme event of sea-level rise along the Northeast coast of North America in 2009–2010

Paul B. Goddard[1], Jianjun Yin[1], Stephen M. Griffies[2] & Shaoqing Zhang[2]

The coastal sea levels along the Northeast Coast of North America show significant year-to-year fluctuations in a general upward trend. The analysis of long-term tide gauge records identified an extreme sea-level rise (SLR) event during 2009–10. Within this 2-year period, the coastal sea level north of New York City jumped by 128 mm. This magnitude of interannual SLR is unprecedented (a 1-in-850 year event) during the entire history of the tide gauge records. Here we show that this extreme SLR event is a combined effect of two factors: an observed 30% downturn of the Atlantic meridional overturning circulation during 2009–10, and a significant negative North Atlantic Oscillation index. The extreme nature of the 2009–10 SLR event suggests that such a significant downturn of the Atlantic overturning circulation is very unusual. During the twenty-first century, climate models project an increase in magnitude and frequency of extreme interannual SLR events along this densely populated coast.

[1] Department of Geosciences, University of Arizona, Tucson, Arizona 85721, USA. [2] Geophysical Fluid Dynamics Laboratory, NOAA, Princeton, New Jersey 08540, USA. Correspondence and requests for materials should be addressed to J.Y. (email: yin@email.arizona.edu).

The Intergovernmental Panel on Climate Change Fifth Assessment Report[1,2] lists extreme sea levels among the top impacts of climate change. Hourly to daily extreme sea levels are typically associated with transient storms and eddies, tides and tsunamis. Once they occur and superimpose, these events pose a threat to coastal communities. On seasonal to interannual time scales, extreme sea-level events are usually linked to large-scale ocean dynamics and climate extremes, but have received little attention thus far.

In the North Atlantic, especially along the Northeast (NE) Coast of North America, sea levels are critically influenced by the Atlantic meridional overturning circulation (AMOC)[3–7]. Since 2004, the AMOC has been systematically monitored at 26.5°N in the North Atlantic[8,9]. The available data reveal a strength of 18.5 ± 1.0 Sv (mean $\pm 1\sigma$) and small interannual variability of the AMOC from 1 April 2004 to 31 March 2009. From April 2009 through March 2010, by contrast, the AMOC shows a significant 30% downturn to 12.8 Sv, followed by a second minimum during the winter of 2010–11 (refs 9–11). Additional observations at other latitudes in the Atlantic indicate that this downturn is a basin-wide phenomenon due to the spatial coherence of the AMOC[12,13].

Whether this downturn of the AMOC is a sign of its long-term trend[14] or a part of its natural variability[11,15], or both[16], will need further research with longer observational data. Regardless, this event provides a valuable opportunity to study the climate impact of the AMOC, quantify the AMOC–sea-level rise (SLR) relationship and test model simulation results. Here we analyse long-term tide gauge (TG) data and report an extreme and unprecedented SLR event in 2009–10 along the NE Coast of North America. It should be noted that we use the term SLR here to indicate interannual sea-level changes, while it is usually referred to the long-term and gradual trend of sea level in literature. With various observation and model data, we show that the 2009–10 SLR event was caused by the 30% downturn of the AMOC and the wind stress anomalies associated with the significant negative North Atlantic Oscillation (NAO) index[17].

Results

TG records. Sea level along the East Coast of the United States and Canada exhibits interannual fluctuations superimposed on multi-decadal variations and a long-term upward trend[5,7,18–20]. Modelling and long-term TG data indicate that the behaviour of sea level is similar and highly correlated north or south of Cape Hatteras[4,5,7,18,20]. By taking the long-term rate and especially the 2009 SLR rate into account (Supplementary Fig. 1), we further divide the East Coast of North America into three SLR regimes: NE (North of New York City), Mid-Atlantic (New York City to Cape Hatteras) and Southeast (south of Cape Hatteras; Fig. 1a). To minimize the effect of local factors and reveal regionally coherent behaviour, we calculate the time series of the sea-level composite for the three SLR regimes (see the Methods section). From the noisy background, we separate an extreme SLR event having occurred between 2009 and 2010 along the NE Coast of North America.

The NE sea-level composite is calculated as the mean of maximum 18 TG stations from Montauk, New York, to Rimouski, Canada (Fig. 1b and Supplementary Table 1). Next, we calculate the yearly SLR rate by differentiating the annual mean time series of the sea-level composite (Fig. 2a) (see the Methods section). The results indicate that the s.d. (σ) of the yearly SLR rate is 14.5 mm per year since 1920, much larger than the secular trend of 2.5 mm per year. However, the composite SLR rate in 2009 is a remarkable outlier and reaches 46.9 mm per year ($>3\sigma$) (Fig. 2b). Between 2009 and 2010, the sea level in this region jumped by nearly 100 mm on average (Figs 1b and 3a), contributing significantly to the identified SLR acceleration during the recent decades[5,7,18]. To calculate the return period, we fit a Gaussian distribution to the yearly SLR rates from 1920 to 2011. The result shows that the 2009 SLR rate is a 1-in-850 year event (Fig. 2c).

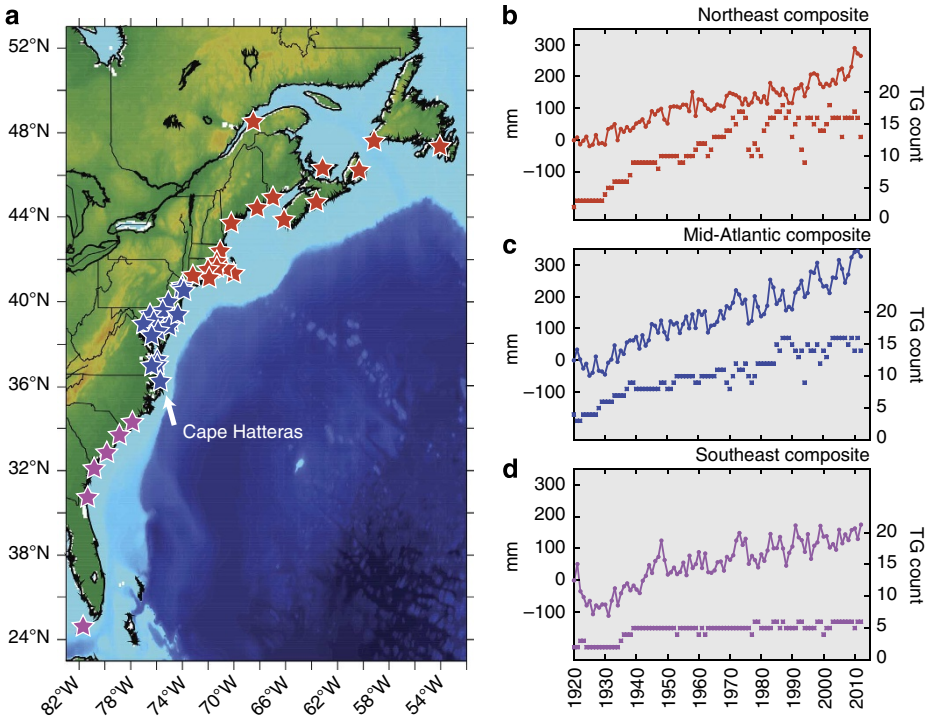

Figure 1 | Three SLR regimes along the East Coast of North America and the corresponding sea-level composite. (**a**) Three SLR regimes and locations of the 40 TG stations used by this study. Red, blue and purple colours indicate the Northeast, Mid-Atlantic and Southeast region, respectively. (**b**–**d**) Time series of sea-level composite (line) in the three regimes and counts of TG stations used in the composite calculation as a function of time (squares).

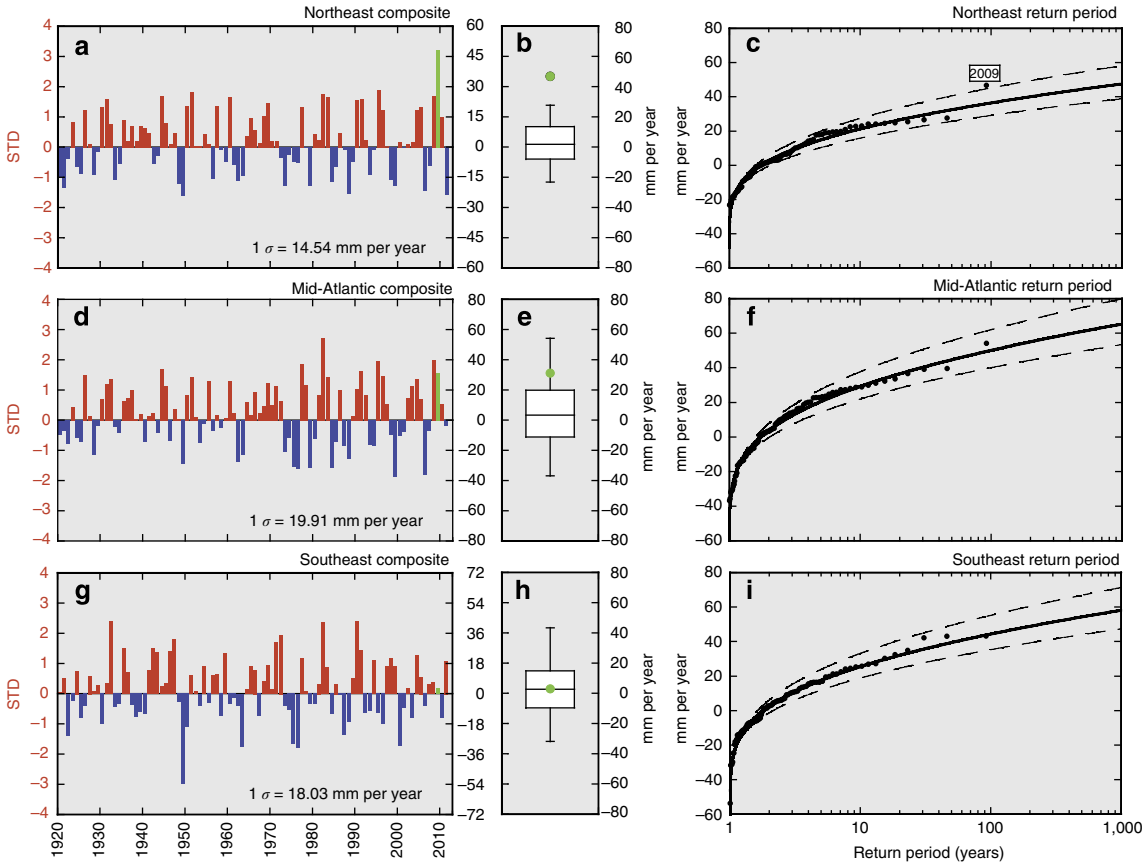

Figure 2 | Yearly SLR rates along the East Coast of North America. (**a**,**d**,**g**) Yearly SLR rates (mm per year) of the Northeast, Mid-Atlantic and Southeast composite, respectively. The absolute and relative (to 1σ) rates are shown by the right and left *y* axis, respectively. (**b**,**e**,**h**) Box and whisker plots indicate the position of the 2009 SLR rates for the three sea-level composites, respectively. The 2009 SLR rates are depicted by the green bars and dots. (**c**,**f**,**i**) Return period of the yearly SLR rates. Dots show the TG data during 1920–2011. Solid lines indicate the exceedance probability of the Gaussian distribution and the corresponding return period. Dotted lines represent the 5%–95% confidence interval of the Gaussian distribution fit. The 2009 box marks the NE 2009 SLR rate. See Methods section for the calculation of the return period.

To test the robustness of the result and its sensitivity to different methods, we repeat the yearly SLR calculation based on the linear fit to the monthly data on interannual time scales (Supplementary Fig. 2). We also identify record-breaking years of sea level and compare the sea-level increase over the previous records (Supplementary Fig. 3). The 2009–10 event stands out in all three methods (Table 1).

The 2009–10 extreme SLR event is also evident in individual TG data (Supplementary Fig. 4). The range of the 2009 SLR rate in the NE region varies from 32.5 (Rimouski) to 64 (Portland) mm per year. Four NE stations (Montauk, Woods Hole, North Sydney and Charlottetown) did not provide data for the calculation of the 2009 SLR rate. Of the remaining 14 stations in the NE region, 11 stations show that the 2009 SLR rate was the highest on record, with the other 3 being the second highest. In addition, the 2009 SLR rate was above 2σ at all NE stations except Rimouski. Five stations (Port-Aux-Basques, Eastport, Halifax, Portland and Boston) show the 2009 SLR rate $>3\sigma$ (Supplementary Fig. 4). The spatial coherency and extreme SLR rate suggest that large-scale ocean climate dynamics (for example, the AMOC[4,21], Gulf Stream[6,22] and wind effect[20,23]) rather than local mechanisms (for example, land subsidence[24]) is the main cause of the 2009 SLR event. Land subsidence is at least one order of magnitude smaller than the yearly SLR rates.

The signal of the 2009–10 extreme SLR event attenuates towards the south. Compared with the NE region, the amplitude of the yearly sea-level fluctuation is larger ($\sigma = 19.9$ mm per year) in the Mid-Atlantic region, while the 2009 SLR rate is less extreme (Fig. 2d,e and Supplementary Fig. 4). The composite SLR rate is 31.2 mm per year ($>1\sigma$) in 2009, with a range of 22.0–41.5 mm per year at individual stations. In the Mid-Atlantic region, especially the Chesapeake Bay, land subsidence induced by glacial isostatic adjustment contributes to the long-term SLR[24]. The pronounced SLR rate during 1982–83 ($>2.5\sigma$ and with a return period of 150 years) is likely related to the strong El Niño in the Pacific and the resulting more coastal storms in the Mid-Atlantic region[23] (Fig. 2d,f).

South of Cape Hatteras, the 2009 SLR rate further reduces to 3.0 mm per year and falls within $\pm 1\sigma$ (Fig. 2g,h). The coastal sea level in this region is influenced by the North Atlantic subtropical gyre[25]. An extreme sea-level fall ($\sim -3\sigma$) occurred in 1949, following a rapid and continuous SLR during much of the 1940s. This decade was characterized by faster global SLR[26]. The detailed investigation about this extreme event is beyond the scope of this study.

The satellite altimetry data indicate that the most significant interannual variability of the dynamic sea level (DSL) occurs in the ocean interior, especially along the Gulf Stream and its extension (Fig. 3a). Along the East Coast of North America, the altimetry data is generally consistent with the TG data regarding the 2009–10 SLR event, but the exact magnitude differs.

Role of the AMOC. The 2009–10 sea-level spike in the NE region coincides with two significant ocean and climate events: a 30%

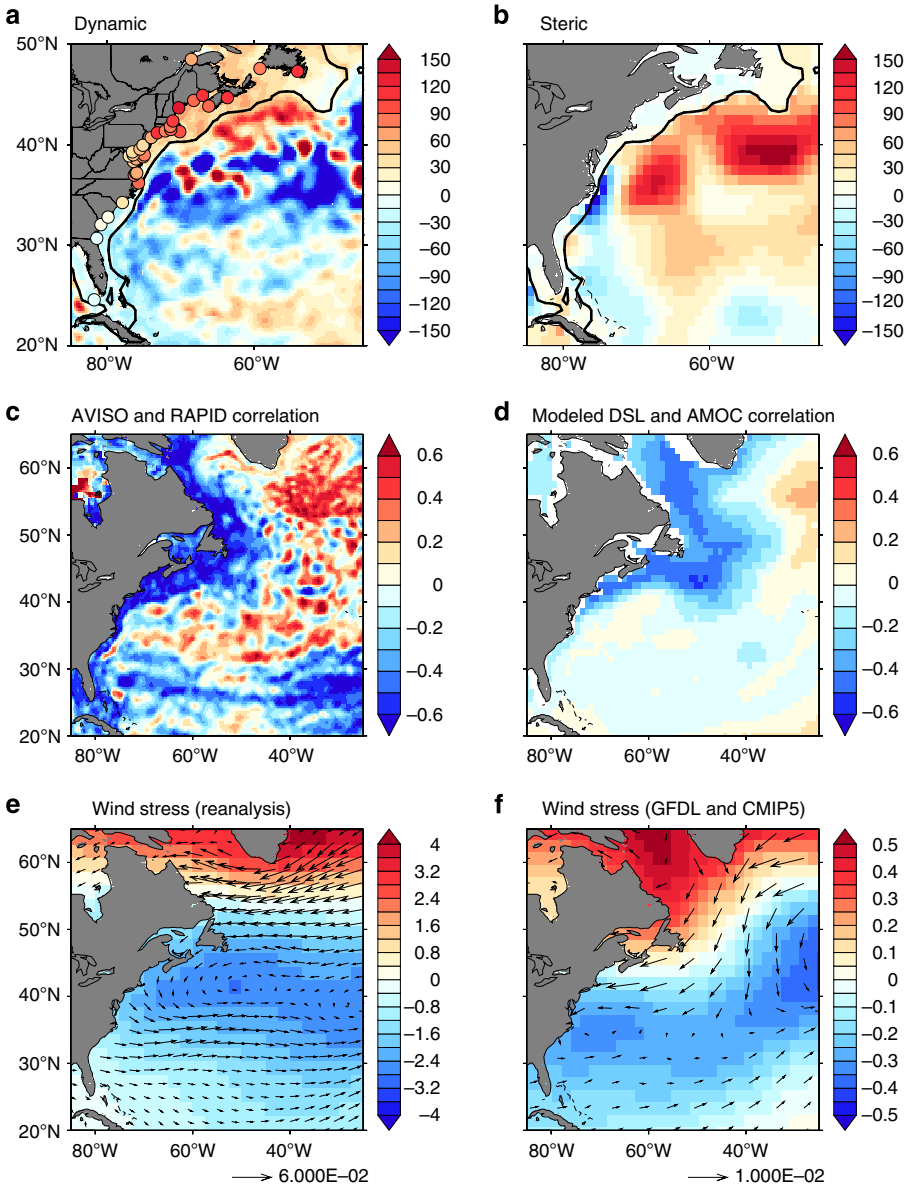

Figure 3 | Mechanisms of the 2009–2010 extreme SLR event. (**a**) Sea-level increase (mm) between 2008 and 2010 from the Archiving, Validation, and Interpretation of Satellite Oceanographic data (AVISO; shading) and TG stations (colour dots). The black line indicates the shelf break—500 m depth. (**b**) Steric sea-level anomalies (mm) in 2009 for the upper 2,000 m. (**c**) Correlation between the monthly AVISO and RAPID AMOC data for 2004–2012. (**d**) Correlation between the annual mean DSL and AMOC index (45°N) in the long-term control runs of the 10 GFDL and 14 CMIP5 models. The values show multi-model ensemble mean. See Supplementary Figs 7 and 8 for individual models. (**e**) Anomalies of sea-level pressure (shading; hPa) and wind stress (vector; $N\,m^{-2}$) in 2009–2010 from the GFDL reanalysis. (**f**) Difference in sea-level pressure (shading; hPa) and wind stress (vector; $N\,m^{-2}$) between the years of extreme positive and negative SLR at Boston. The results show the ensemble mean of the GFDL and CMIP5 models for 100-year control runs. See Supplementary Figs 10 and 11 for more details.

downturn of the AMOC[9] (Fig. 4a) and an extreme negative NAO index[27]. Both winds[20,23,25] and the AMOC[4,5,18,21] can cause sea-level variability and change along the NE coast of North America on various time scales. After removing the seasonal cycle, the monthly NE sea-level composite shows a good correlation ($R = 0.78$; 2-month lag) with the AMOC index (Fig. 4b). Especially, the two sea-level spikes during the winters of 2009–10 and 2010–11 coincide with the two AMOC minima, respectively. Regression based on all monthly data from 2004 to 2012 further reveals a 13.2-mm SLR along the NE coast in response to 1 Sv AMOC slowdown. After excluding the 30% downturn period of the AMOC, the AMOC-SLR ratio increases to 16.6 mm Sv^{-1}, reflecting the sea-level response to the gradual decline of the AMOC during 2004–2012. In the altimetry data, the AMOC–DSL correlation extends far offshore, especially from the NE coast of North America (Fig. 3c). It changes sign across the Gulf Stream, implying that a decrease in the AMOC transport reduces the cross-current sea-level gradient and thus lifts sea level along the NE coast[5,6].

Interestingly, the 30% downturn of the AMOC in 2009–2010 followed a brief return to deep convection in the Labrador Sea during the winter of 2007–2008 (ref. 28). A data assimilation product by GFDL[29,30] (see the Methods section) shows that strong deep downwelling in 2007–2008 was mainly induced by a reduction in the freshwater input into the Labrador Sea (Supplementary Fig. 5). However, a record low of oceanic

Table 1 | Summary of the rise rates in the three SLR regimes.

	Northeast	Mid-Atlantic	Southeast
Sea level differentiation method for yearly SLR rate			
s.d. (mm per year)	14.5	19.9	18.0
2009 Rate (mm per year)	46.9	31.2	3.0
Range of the 2009 rate at different stations (mm per year)	32.5–64.0	22.0–41.5	−7–16
Linear fit method for yearly SLR rate			
s.d. (mm per year)	14.1	20.3	17.7
2009 Rate (mm per year)	41.7	31.2	13.5
2009 Error bar (mm per year)	8.6	12.0	16.1
2010 Sea-level increase over previous record (mm)	59.4	17.1	—
Long-term trend (1920–2012) (mm per year)	2.5	3.5	2.3

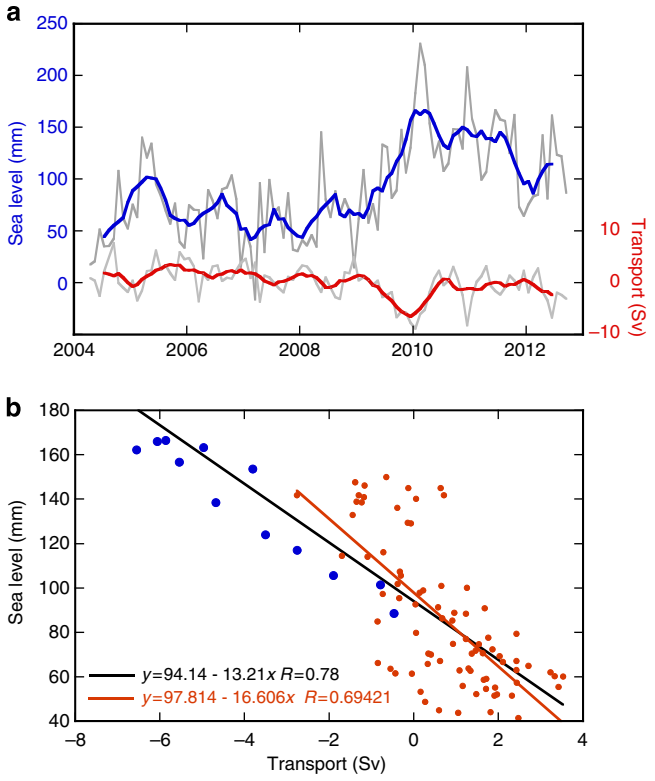

Figure 4 | Correlation between the AMOC and the sea-level composite along the NE coast. (**a**) The time series of the NE sea-level composite (monthly grey, filtered blue) and the AMOC strength at 26.5°N (Sv, monthly grey, filtered red). The seasonal cycle has been removed with a 6-month filter applied. (**b**) The monthly correlation and regression between the AMOC and NE sea-level composite (mm per Sv, 2-month lag with the AMOC leading the SLR). The blue dots highlight the data during the period of the 30% AMOC downturn. The linear fit in black is based on all monthly data during April 2004–September 2012. The linear fit in red is based on the red dots only and excluding the period of the 30% AMOC downtown. The data are from PSMSL and the RAPID-WATCH MOC project.

heat and buoyancy loss, dominated by the sensible heat flux (Supplementary Fig. 6), occurred in the subsequent years 2008–2010. Associated with these changes is a significant positive steric sea-level anomaly in 2009 (>100 mm), southeastward of the shelf break (Fig. 3b). The gradient across the shelf break can drive more water mass towards the shelf, thereby causing SLR along the NE coast of North America[4,31].

To better understand extreme SLR events in this region, we use two sets of state-of-the-art climate models: an ensemble of ten

Table 2 | Ten global climate/Earth system models developed at GFDL and used in this study.

Model	Atmosphere	Ocean	Documentation
CM2.6	0.5°	0.1°, z* coordinate	Delworth *et al.*[44] Griffies *et al.*[32] Winton *et al.*[45]
CM2.5	0.5°	0.25°, z* coordinate	Delworth *et al.*[44] Griffies *et al.*[32] Winton *et al.*[45]
CM2.5FLORa6	0.5°	1°, z* coordinate	Vecchi *et al.*[46] Griffies *et al.*[32] Winton *et al.*[45]
CM2.5FLOR	0.5°	1°, z* coordinate	Vecchi *et al.*[46] Griffies *et al.*[32] Winton *et al.*[45]
CM2.0	2°	1°, z coordinate	Delworth *et al.*[47]
CM2.1	2°	1°, z coordinate	Delworth *et al.*[47]
CM3	2°	1°, z* coordinate	Griffies *et al.*[48]
ESM2M	2°	1°, z* coordinate	Dunne *et al.*[49]
ESM2preG	2°	1°, Isopycnal	Dunne *et al.*[49]
ESM2G	2°	1°, Isopycnal	Dunne *et al.*[49]

models developed at GFDL, including high-resolution models with eddying oceans[32] (Table 2), and the other set including 14 CMIP5 models with the AMOC and sea-level data available at the CMIP5 archive[33] (Table 3; also see the Methods section). The GFDL ensemble represents different model generations with progressive improvement and a systematic model development effort at one modelling centre. On the other hand, the CMIP5 ensemble represents similar generation models from different institutes, which bear significant difference in many aspects. Therefore, these models cover a wide range in the model formulation, parameterization and uncertainty space.

In the long-term control runs of these models without changing external forcing, the DSL along the NE coast of North America shows an instantaneous correlation with the AMOC on the interannual time scale (Fig. 3d and Supplementary Figs 7 and 8). This correlation suggests that a 30% weakening of the AMOC in 2009–2010 may have contributed to and increased the chance of extreme coastal SLR events. The two models with eddying oceans (GFDL CM2.6 and CM2.5) show weaker correlation, probably due to the relatively weak AMOC in these two models[32] (Supplementary Fig. 9).

Role of the NAO and associated winds. The significant negative NAO index during December 2009 through February 2010 (ref. 27) contributes to the extreme SLR event both remotely and locally. First, the negative NAO can cause an anomalous heat flux

Table 3 | 14 CMIP5 global climate/Earth system models used in this study.

Model	Institution
ACCESS1.0	Commonwealth Scientific and Industrial Research Organisation, Australia
ACCESS1.3	Commonwealth Scientific and Industrial Research Organisation, Australia
CCSM4	National Center for Atmospheric Research, USA
CESM1-BGC	National Center for Atmospheric Research, USA
CESM1-FASTCHEM	National Center for Atmospheric Research, USA
CESM1-WACCM	National Center for Atmospheric Research, USA
CMCC-CM	Centro Euro-Mediterraneo sui Cambiamenti Climatici, Italy
INM-CM4	Institute of Numerical Mathematics, Russia
MPI-ESM-LR	Max Planck Institute for Meteorology, Germany
MPI-ESM-MR	Max Planck Institute for Meteorology, Germany
MPI-ESM-P	Max Planck Institute for Meteorology, Germany
MRI-CGCM3	Meteorological Research Institute, Japan
NorESM1-M	Norwegian Climate Center, Norway
NorESM1-ME	Norwegian Climate Center, Norway

into the Labrador Sea, thereby influencing the AMOC and SLR along the NE coast of North America (Supplementary Fig. 5). Second, the NAO-induced wind stress anomalies can pile up waters directly against the NE coast or generate onshore Ekman transport.

The control runs with both the GFDL and other CMIP5 models indicate that extreme SLR events along the NE coast typically occur when the nearby wind stress shows an onshore (easterly) or alongshore (northeasterly) anomaly pattern (Fig. 3f and Supplementary Figs 10 and 11). Indeed, the lower sea-level pressure east of North America in 2009 results in northeasterly wind stress anomalies near the NE coastal regions (Fig. 3e). The anomalous Ekman transport contributes to the 2009–2010 SLR extreme. The negative NAO can also influence storminess, which contributes to higher sea levels due to more frequent storm surges[34].

The NE sea-level composite shows correlation ($R = 0.6$) with the NAO index during 2004–2012 (Supplementary Fig. 12). However, the correlation reduces significantly for the entire period of 1920–2012. In addition to 2009–2010, extreme negative NAO index also occurred in 1969 and other years (Supplementary Fig. 13). The lack of extreme SLR signal on the NE coast during these years indicates that the NAO is not the sole mechanism of the 2009–2010 SLR event. Finally, the lower sea-level pressure (by $\sim$1.6 hPa) in 2009 could account for $\sim$15% of the 2009–10 SLR event through the inverse barometer effect (Fig. 3e).

Future projections of extreme SLR events. Similar to extreme temperature and precipitation events, extreme SLR events on the interannual time scale may be also linked to human-induced climate change[35]. Increased greenhouse gas concentrations are likely to shift the probability density function towards more extremes. To study future changes of extreme SLR events, we consider the ten GFDL climate models and their long-term control runs, and idealized 1% per year CO_2 increase experiments for 100 years. Along the NE coast of North America, most of these models (CM2.6, CM2.5, CM2.5 FLORa6, CM2.5 FLOR, ESM2M and ESM2preG) suggest an increase in the magnitude and frequency of the extreme SLR events in response to the CO_2 increase (Fig. 5 and Supplementary Fig. 14). In five of these models (CM2.6, CM2.5 FLORa6, CM2.5 FLOR, ESM2M and ESM2preG), the increase in the yearly SLR extrema is unproportionately larger than the increase in mean sea level (Supplementary Fig. 14).

There are several reasons for this increase in extremes: first, the global mean SLR from thermal expansion and land ice melt (note that the latter is not included in Fig. 5); second, the overall weakening of the AMOC in the CO_2 experiment leads to record lows of the circulation in some years (Supplementary Fig. 9), thereby facilitating SLR extremes along the NE coast of North America; and third, the NAO variability remains strong in the CO_2 experiments[36]. Recently, projections of the melting of glaciers[37], the Greenland[38] and Antarctic[39] ice sheets, have been made for the twenty-first century under greenhouse gas emission scenarios. Adding these contributions would further increase the probability of extreme SLR events along the East Coast of North America, especially its northeastern sector.

Discussion

In the present study, we focus on the extreme SLR event on interannual time scales. With long-term TG data, we calculate the sea-level composite and yearly SLR rates for three SLR regimes along the East Coast of North America. The resulting time series contain rich information about both climate variability and individual events. The extreme and unprecedented SLR event in 2009–2010 is particularly notable along the NE coast of North America. Our analysis suggests that this event was mainly caused by a 30% downturn of the AMOC and the wind stress anomalies associated with the negative NAO, although the two factors are inherently linked[17].

There is no direct observation of the AMOC before 2004. Some recent model hindcast suggests that similar downturns of the AMOC may have punctuated in the twentieth century[11]. Our analysis based on the long-term TG data and the AMOC–SLR relationship indicates that the 2009–2010 event is very unusual. In addition to internal variability, anthropogenic forcing could be another impact factor, as most climate models project a weakening of the AMOC during the twenty-first century in response to the increase in the atmospheric greenhouse gas concentrations[40]. Continuing observations of the AMOC is essential to confirm these modelling results.

In addition to the absolute SLR rate, the 2009–2010 event is very unusual also in the sense that it occurred during a short period of global sea-level fall[41]. Unlike storm surge, this event caused persistent and widespread coastal flooding[22] even without apparent weather processes. In terms of beach erosion, the impact of the 2009–2010 SLR event is almost as significant as some hurricane events[42]. For the twenty-first century, modelling results suggest that the increase in the greenhouse gas concentrations is likely to cause more extreme SLR events on the interannual time scale along this densely populated coast. Once coastal storms compound high sea levels, more damages will result.

Methods

TG data. The data are selected from the Permanent Service for Mean Sea Level global database for TG records[43] (http://www.psmsl.org/data/obtaining). We selected records with at least 25 years and 70% completeness that were up to date through 2012. This method provides 40 TG stations along the East Coast from Key West, Florida, to Rimouski, Canada (Supplementary Table 1).

Satellite altimetry data. For the absolute DSL, we use the Archiving, Validation, and Interpretation of Satellite Oceanographic data. This delayed time data set provides 1/4° × 1/4° resolution in daily intervals from 1 January 1993 through 31 December 2012 (http://www.aviso.altimetry.fr/en/data/data-access.html).

AMOC time series. For *in-situ* observations of the AMOC, we use the data from the RAPID-WATCH MOC monitoring project (http://www.rapid.ac.uk/rapidmoc). This data set has a twice per day temporal resolution and ranges from April 2004 through October 2012 (at the time of download).

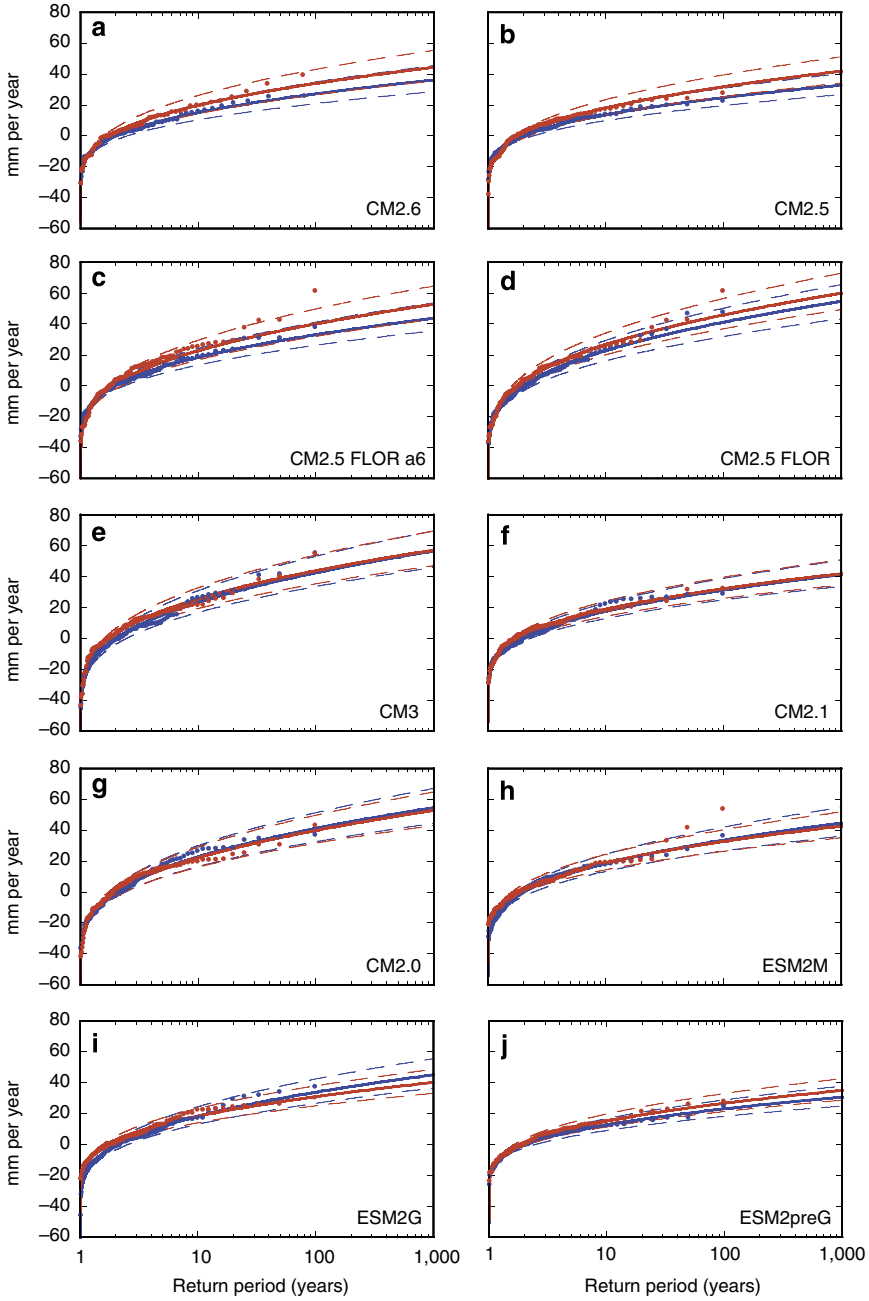

Figure 5 | Return periods of the yearly SLR rates in the control runs and 1% per year CO_2 increase experiments with the ten GFDL models. The values show the composite SLR rates along the NE Coast of North America and are calculated based on both the DSL changes and the global ocean thermal expansion. Both the control (blue colour) and CO_2 runs (red colour) are 100-year long. Dots show the model simulation results. Solid lines indicate the exceedance probability of the Gaussian distribution and the corresponding return period. Dotted lines represent the 5%–95% confidence interval of the Gaussian distribution fit. The red line above the blue line indicates an increase in the return level or a decrease in the return period.

Yearly SLR rate. We differentiate the sea-level time series to obtain the yearly SLR rates.

$$\mathrm{SLR}(t) = \frac{\mathrm{SL}(t+1) - \mathrm{SL}(t-1)}{2}, \quad t = \text{second record,....2011} \qquad (1)$$

SLR(t) is the SLR rate (mm per year) for a particular year, and SL($t+1$) and SL($t-1$) denote the sea-level records for the previous and next year, respectively. It should be noted that six TG stations are not included in calculating the 2009 SLR rate due to missing data for 2008 or 2010. The results are compared with those based on the linear fit (Supplementary Fig. 2).

Return period. Based on the millennial time-scale control simulations of the ten GFDL models (not shown), we find the yearly SLR rates are well fitted with a Gaussian distribution. For a return level x_t, the probability of exceedance is $Pr(x > x_t)$, where Pr is the cumulative density function associated with the Gaussian distribution. The return period (T) is calculated as $T = 1/Pr$.

GFDL ocean data assimilation data. The GFDL ocean data assimilation data are taken from the oceanic component of climate reanalysis by coupled data assimilation[30]. We use longwave (LW), shortwave (SW), sensible heat (SH), latent heat (LH), precipitation minus evaporation (P − E), and river runoff (R) fluxes from the GFDL climate reanalysis product[29], where Q_{HF} (W m^{-2}) and Q_{WF} (m s^{-1}) are the net atmosphere–ocean heat (positive values indicate flux into ocean) and freshwater flux, respectively.

$$Q_{HF} = \mathrm{LW} + \mathrm{SW} + \mathrm{SH} + \mathrm{LH} \qquad (2)$$

$$Q_{WF} = (\mathrm{P} - \mathrm{E} + \mathrm{R}) \qquad (3)$$

Ocean temperature, salinity and steric sea-level data. We use the data from the National Oceanographic Data Center (http://www.nodc.noaa.gov/OC5/3M_HEAT_CONTENT/). The steric sea-level anomaly data for the upper 2,000 m span from 2005–2013.

GFDL model suite. We consider ten coupled climate models built over the past decade at GFDL (Table 2). CM2.0 and CM2.1 were used as part of the CMIP3 projects, whereas CM3 and ESM2M/ESM2G were used as part of the CMIP5 project. ESM2preG is an early version of ESM2G. Each of these models uses a nominally 1° ocean, with various changes made to the atmosphere and ocean components, leading to the different configurations. Notably, the ESM2G and ESM2preG are based on an isopycnal ocean, whereas the other models use a level coordinate MOM ocean component. CM2.6, CM2.5, CM2.5 FLORa6 and CM2.5 FLOR all use the same 50-km finite volume atmospheric core, with CM2.6 using a 1/10° ocean, CM2.5 a 1/4° ocean and the FLOR simulations using a 1° ocean. The two FLOR simulations differ in their choice for ocean subgrid scale parameterizations, with FLORa6 using a larger lateral viscosity than FLOR. CM2.5 FLOR is used for studies of tropical cyclones.

CMIP5 model suite. The data are downloaded from the CMIP5 archive[33] (Table 3). Detailed model description and experimental design can be found at http://cmip-pcmdi.llnl.gov/cmip5/.

References

1. Church, J. A. *et al.* in *Climate Change 2013: The Physical Science Basis* (eds Stocker, T. F. *et al.*) (Cambridge University Press, 2013).
2. Wong, P. P. *et al.* in *Climate Change 2014: Impacts, Adaptation, and Vulnerability. Part A: Global and Sectoral Aspects. Contribution of Working Group II to the Fifth Assessment Report of the Intergovernmental Panel on Climate Change* (eds Field, C. B. *et al.*) (Cambridge University Press, 2014).
3. Levermann, A., Griesel, A., Hofmann, M., Montoya, M. & Rahmstorf, S. Dynamic sea level changes following changes in the thermohaline circulation. *Clim. Dyn.* **24,** 347–354 (2005).
4. Yin, J., Schlesinger, M. E. & Stouffer, R. J. Model projections of rapid sea-level rise on the northeast coast of the United States. *Nat. Geosci.* **2,** 262–266 (2009).
5. Sallenger, A. H., Doran, K. S. & Howd, P. A. Hotspot of accelerated sea-level rise on the Atlantic coast of North America. *Nat. Clim. Change* **2,** 884–888 (2012).
6. Ezer, T., Atkinson, L. P., Corlett, W. B. & Blanco, J. L. Gulf Stream's induced sea level rise and variability along the U.S. mid-Atlantic coast. *J. Geophys. Res.* **118,** 685–697 (2013).
7. Boon, J. D. Evidence of sea level acceleration at U.S. and Canadian tide stations, Atlantic Coast, North America. *J. Coast. Res.* **28,** 1437–1445 (2012).
8. Cunningham, S. A. *et al.* Temporal variability of the Atlantic meridional overturning circulation at 26.5 degrees N. *Science* **317,** 935–938 (2007).
9. McCarthy, G. D. *et al.* Observed interannual variability of the atlantic meridional overturning circulation at 26.5°N. *Geophys. Res. Lett.* **39,** L19609 (2012).
10. Smeed, D. A. *et al.* Observed decline of the Atlantic meridional overturning circulation 2004–2012. *Ocean Sci.* **10,** 29–38 (2014).
11. Blaker, A. T. *et al.* Historical analogues of the recent extreme minima observed in the Atlantic meridional overturning circulation at 26° N. *Clim. Dyn.* **44,** 457–473 (2014).
12. Rhein, M. *et al.* in *Climate Change 2013: The Physical Science Basis. Contribution of Working Group I to the Fifth Assessment Report of the Intergovernmental Panel on Climate Change* (eds Stocker, T. F. *et al.*) (Cambridge University Press, 2013).
13. Newlin, I. L. & Gregg, M. C. Global Oceans [in 'State of the Climate in 2013']. *Bull. Am. Meteorol. Soc.* **95,** s51–s78 (2014).
14. Robson, J., Hodson, D., Hawkins, E. & Sutton, R. Atlantic overturning in decline? *Nat. Geosci.* **7,** 2–3 (2014).
15. Roberts, C. D., Jackson, L. & McNeall, D. Is the 2004–2012 reduction of the Atlantic meridional overturning circulation significant? *Geophys. Res. Lett.* **41,** 3204–3210 (2014).
16. Schiermeier, Q. OCEANOGRAPHY Atlantic current strength declines. *Nature* **509,** 270–271 (2014).
17. Bryden, H. L., King, B. A., McCarthy, G. D. & McDonagh, E. L. Impact of a 30% reduction in Atlantic meridional overturning during 2009–2010. *Ocean Sci.* **10,** 683–691 (2014).
18. Ezer, T. Sea level rise, spatially uneven and temporally unsteady: Why the US East Coast, the global tide gauge record, and the global altimeter data show different trends. *Geophys. Res. Lett.* **40,** 5439–5444 (2013).
19. Kopp, R. E. Does the mid-Atlantic United States sea level acceleration hot spot reflect ocean dynamic variability? *Geophys. Res. Lett.* **40,** 3981–3985 (2013).
20. Andres, M., Gawarkiewicz, G. G. & Toole, J. M. Interannual sea level variability in the western North Atlantic: regional forcing and remote response. *Geophys. Res. Lett.* **40,** 5915–5919 (2013).
21. Yin, J. & Goddard, P. B. Oceanic control of sea level rise patterns along the East Coast of the United States. *Geophys. Res. Lett.* **40,** 5514–5520 (2013).
22. Sweet, W., Zervas, C. & Gill, S. *Elevated East Coast Sea Level Anomaly: June-July 2009*. NOAA Technical Report NOS CO-OPS 051, 40pp (NOAA Natl. Ocean Service, Silver Spring, MD, USA, 2009).
23. Sweet, W. V. & Zervas, C. Cool-season sea level anomalies and storm surges along the US east coast: climatology and comparison with the 2009/10 El Nino. *Mon. Wea. Rev.* **139,** 2290–2299 (2011).
24. Boon, J. D., Brubaker, J. & Forrest, D. R. *Chesapeake Bay Land Subsidence and Sea Level Change: An Evaluation of Past and Present Trends and Future Outlook* (Virginia Institute of Marine Science, 2010).
25. Hong, B. G., Sturges, W. & Clarke, A. J. Sea level on the US East Coast: decadal variability caused by open ocean wind-curl forcing. *J. Phys. Oceanogr.* **30,** 2088–2098 (2000).
26. Church, J. A. & White, N. J. Sea-level rise from the late 19th to the early 21st century. *Surv. Geophys.* **32,** 585–602 (2011).
27. Hu, Z. Z. *et al.* Persistent atmospheric and oceanic anomalies in the North Atlantic from summer 2009 to summer 2010. *J. Clim.* **24,** 5812–5830 (2011).
28. Vage, K. *et al.* Surprising return of deep convection to the subpolar North Atlantic Ocean in winter 2007–2008. *Nat. Geosci.* **2,** 67–72 (2009).
29. Chang, Y.-S., Zhang, S., Rosati, A., Delworth, T. L. & Stern, W. F. An assessment of oceanic variability for 1960–2010 from the GFDL ensemble coupled data assimilation. *Clim. Dyn.* **40,** 775–803 (2013).
30. Zhang, S., Harrison, M. J., Rosati, A. & Wittenberg, A. System design and evaluation of coupled ensemble data assimilation for global oceanic climate studies. *Mon. Wea. Rev.* **135,** 3541–3564 (2007).
31. Griffies, S. M. *et al.* An assessment of global and regional sea level for years 1993-2007 in a suite of interannual CORE-II simulations. *Ocean Model.* **78,** 35–89 (2014).
32. Griffies, S. M. *et al.* Impacts on ocean heat from transient mesoscale eddies in a hierarchy of climate models. *J. Clim.* doi:10.1175/JCLI-D-14-00353.1 (2015).
33. Taylor, K. E., Stouffer, R. J. & Meehl, G. A. An overview of CMIP5 and the experiment design. *Bull. Am. Meteorol. Soc.* **93,** 485–498 (2012).
34. Ezer, T. & Atkinson, L. P. Accelerated flooding along the US East Coast: on the impact of sea-level rise, tides, storms, the Gulf Stream, and the North Atlantic oscillations. *Earth Future* **2,** 362–382 (2014).
35. Field, C. B. *Managing the Risks of Extreme Events and Disasters to Advance Climate Change Adaptation: Special Report of the Intergovernmental Panel on Climate Change* (Cambridge University Press, 2012).
36. Christensen, J. H. *et al.* in *Climate Change 2013: The Physical Science Basis. Contribution of Working Group I to the Fifth Assessment Report of the Intergovernmental Panel on Climate Change* (eds Stocker, T. F. *et al.*) (Cambridge University Press, 2013).
37. Marzeion, B., Jarosch, A. H. & Hofer, M. Past and future sea-level change from the surface mass balance of glaciers. *Cryosphere* **6,** 1295–1322 (2012).
38. Fettweis, X. *et al.* Estimating the Greenland ice sheet surface mass balance contribution to future sea level rise using the regional atmospheric climate model MAR. *Cryosphere* **7,** 469–489 (2013).
39. Levermann, A. *et al.* Projecting Antarctic ice discharge using response functions from SeaRISE ice-sheet models. *Earth Syst. Dyn.* **5,** 271–293 (2014).
40. Weaver, A. J. *et al.* Stability of the Atlantic meridional overturning circulation: a model intercomparison. *Geophys. Res. Lett.* **39,** L20709 (2012).
41. Boening, C., Willis, J. K., Landerer, F. W., Nerem, R. S. & Fasullo, J. The 2011 La Nina: so strong, the oceans fell. *Geophys. Res. Lett.* **39,** L19602 (2012).
42. Theuerkauf, E. J., Rodriguez, A. B., Fegley, S. R. & Luettich, R. A. Sea level anomalies exacerbate beach erosion. *Geophys. Res. Lett.* **41,** 5139–5147 (2014).
43. Holgate, S. J. *et al.* New data systems and products at the permanent service for mean sea level. *J. Coast. Res* **29,** 493–504 (2013).
44. Delworth, T. L. *et al.* Simulated climate and climate change in the GFDL CM2. 5 high-resolution coupled climate model. *J. Clim.* **25,** 2755–2781 (2012).
45. Winton, M. *et al.* Has coarse ocean resolution biased simulations of transient climate sensitivity? *Geophys. Res. Lett.* **41,** 8522–8529 (2014).
46. Vecchi, G. *et al.* On the seasonal forecasting of regional tropical cyclone activity. *J. Clim.* **27,** 7994–8016 (2014).
47. Delworth, T. L. *et al.* GFDL's CM2 global coupled climate models. Part I: formulation and simulation characteristics. *J. Clim.* **19,** 643–674 (2006).
48. Griffies, S. M. *et al.* The GFDL CM3 coupled climate model: characteristics of the ocean and sea ice simulations. *J. Clim.* **24,** 3520–3544 (2011).
49. Dunne, J. P. *et al.* GFDL's ESM2 global coupled climate-carbon Earth System Models Part I: physical formulation and baseline simulation characteristics. *J. Clim.* **25,** 6646–6665 (2012).

Acknowledgements

We thank Drs R. Stouffer and M. Winton for constructive comments. We thank Dr M. Winton for providing simulations of the ten GFDL models, and many research centres for providing the observation and modelling data. The work was supported by the NOAA Climate Program Office (grant number NA13OAR4310128).

Author contributions

P.G. and J.Y. designed the study, analysed the data and wrote the manuscript. S.M.G. provided the data and information of the ten GFDL models. S.Z. provided the GFDL reanalysis data. All authors made contributions to data interpretation and manuscript writing.

Additional information

Supplementary Information accompanies this paper at http://www.nature.com/naturecommunications

Competing financial interests: The authors declare no competing financial interests.

Reprints and permission information is available online at http://npg.nature.com/reprintsandpermissions/

How to cite this article: Goddard, P. B. *et al.* An extreme event of sea-level rise along the Northeast coast of North America in 2009–2010. *Nat. Commun.* 6:6346 doi: 10.1038/ncomms7346 (2015).